Available online at www.sciencedirect.com
ScienceDirect
Journal of Power Sources 172 (2007) 39–49
JOURNAL OF POWER SOURCES
www.elsevier.com/locate/jpowsour

Polarization measurements on single-step co-fired solid oxide fuel cells (SOFCs)

Kyung Joong Yoon, Peter Zink, Srikanth Gopalan *, Uday B. Pal

Department of Manufacturing Engineering, Boston University, Boston, MA 02215, USA

Received 29 October 2006; received in revised form 11 February 2007; accepted 2 March 2007
Available online 12 March 2007

Abstract

Anode-supported planar solid oxide fuel cells (SOFC) were successfully fabricated by a single step co-firing process. The cells comprised of a Ni + yttria-stabilized zirconia (YSZ) anode, a YSZ or scandia-stabilized zirconia (ScSZ) electrolyte, a $(La_{0.85}Ca_{0.15})_{0.97}MnO_3$ (LCM) + YSZ cathode active layer, and an LCM cathode current collector layer. The fabrication process involved tape casting of the anode, screen printing of the electrolyte and the cathode, and single step co-firing of the green-state cells in the temperature range of 1300–1330 °C for 2 h. Cells were tested in the temperature range of 700–800 °C with humidified hydrogen as fuel and air as oxidant. Cell test results and polarization modeling showed that the polarization losses were dominated by the ohmic loss associated with the electrodes and the activation polarization of the cathode, and that the ohmic loss due to the ionic resistance of the electrolyte and the activation polarization of the anode were relatively insignificant. Ohmic resistance associated with the electrode was lowered by improving the electrical contact between the electrode and the current collector. Activation polarization of the cathode was reduced by the improvement of the microstructure of the cathode active layer and lowering the cell sintering temperature. The cell performance was further improved by increasing the porosity in the anode. As a result, the maximum power density of 1.5 W cm^{-2} was achieved at 800 °C with humidified hydrogen and air.

Keywords: Fuel cells; Solid oxide; Single-step co-fired; Polarization; Cathode; Anode; Solid electrolyte

1. Introduction

Solid oxide fuel cells (SOFCs) have gained significant interest due to their high-energy conversion efficiency, low pollution emission, and flexibility with various fuels. Among the basic designs of SOFCs, the anode-supported SOFCs are extensively investigated because they exhibit higher cell performance compared to either the electrolyte-supported or cathode-supported designs. Maximum power densities of 1.8–1.9 W cm^{-2} at 800 °C have been reported using an anode-supported design [1–3].

The major challenge for the commercialization of SOFCs is reducing the high manufacturing costs. Currently, the production cost of batch-processed SOFCs is significantly higher than that of conventional power generation systems. Therefore, in recent years, enormous research efforts have been directed at the development of a commercially viable SOFC fabrication technology. Conventional SOFC fabrication technologies involve multiple sintering steps for a single cell fabrication, and the sintering step is one of the most expensive processes during cell fabrication. Therefore, reducing the number of sintering steps in the SOFC fabrication process can greatly lower the manufacturing costs. To realize the successful single step co-firing of SOFCs, it is critical to lower the sintering temperature of the electrolyte, and to minimize the thermal expansion mismatch and sintering shrinkage mismatch between the components. Lowering the electrolyte sintering temperature allows co-firing of the entire cell, while at the same time maintaining sufficient connected porosity in the anode and the cathode, which is critical for the transport of reactant and product gases. Furthermore, chemical interactions between the components are minimized by lowering the firing temperature. For the co-firing of a multi-layer SOFC structure, it is also very important to minimize the cell camber which occurs due to thermal expansion mismatch and sintering shrinkage mismatch between the individual components. This requires careful matching of the thermal expansion

* Corresponding author. Tel.: +1 6173582297; fax: +1 6173535548.
E-mail address: sgopalan@bu.edu (S. Gopalan).

0378-7753/$ – see front matter © 2007 Elsevier B.V. All rights reserved.
doi:10.1016/j.jpowsour.2007.03.003

coefficients and sintering shrinkages of the individual layers. The sintering temperature, the amount of pore former and other additives influence the sintering shrinkage of the components. Initial experiments focused on measuring the sintering shrinkage of the individual components by varying these factors. A camber-free flat cell can be achieved by matching the sintering shrinkage of the individual components through an engineering optimization of these factors [4].

In the present work, anode-supported planar SOFCs were fabricated by a single step co-firing process. Fabrication processes involved tape casting of the anode, screen printing of the electrolyte and the cathode, and a single step co-firing of the green-state cells at 1300–1330 °C [4]. The fabricated cells were tested in the temperature range between 700 °C and 800 °C with humidified hydrogen as fuel and air as oxidant. DC polarization curves (voltage–current density plots) were obtained from the cells, and the cells were also characterized using AC impedance spectroscopy. Experimentally measured voltage versus current density traces were fitted into a polarization model, and the voltage drops of the cells were separated into various polarization losses using the model. The effects of various process parameters on the polarization and the performance of the cells are discussed.

2. Experimental

2.1. Conductivity measurements of electrolyte materials

Rectangular bars for electrical conductivity measurements were prepared with commercially purchased ScSZ (10 mol% Sc_2O_3–1 mol% CeO_2–89 mol% ZrO_2) (Sumitomo) and YSZ (8 mol% Y_2O_3–92 mol% ZrO_2) (Tosoh Corp.) powders with and without sintering aids. A 0.2 mol% of aluminum oxide (Alfa Aesar) was used as a sintering aid. The electrical conductivity was measured by a four-probe DC measurement technique at 800 °C, 750 °C, and 700 °C.

2.2. Cell fabrication

The cells used in the present work were fabricated by the single-step co-firing process shown in Fig. 1. Commercially purchased NiO (J.T. Baker) and 8 mol% YSZ (Tosoh Corp.) powders were mixed in ethanol and toluene with the desired amounts of pore former (Carbon black, Fisher Scientific), binder (Polyvinyl butyral, Butvar), dispersant (LP1, Heraeus), and plasticizer (Benzyl-butyl phthalate, Alpha Aesar) for 4 h. The average particle size of NiO and YSZ was ∼0.8 μm and ∼0.2 μm, respectively, and the weight ratio between NiO and YSZ was 1.9:1. After mixing, anode tapes were formed by tape casting. The tapes were cut into disc-shaped samples and laminated to form ∼1 mm thick anode supports. The electrolyte slurry was prepared by mixing YSZ or ScSZ powders and 0.2 mol% of the sintering aid in alpha-terpineol (Alfa Aesar) with binder (V6, Heraeus) for 4 h, which was applied over the anode support by screen printing. For the preparation of slurry for the cathode active layer, LCM powder was prepared by mixing precursors of lanthanum carbonate (Alfa Aesar), calcium oxide (Alfa Aesar), and manganese oxide (Alfa Aesar) and calcining at 1400 °C for 4 h. Then, LCM and YSZ powders were mixed in a 1:1 weight ratio and milled for 10 h in alpha-terpineol with the desired amount of pore former (Carbon black, Fisher Scientific) and binder (V6, Heraeus). The average particle size of the LCM powder was ∼1.0 μm. After mixing, the cathode active layer was screen-printed on top of the electrolyte layer. Slurry for the cathode current collector was prepared by mixing LCM powder with the desired amount of pore former (Carbon black, Fisher Scientific) and binder (V6, Heraeus) in alpha-terpineol. The slurry was then applied on top of the cathode active layer by screen printing. The sintering shrinkage of each component was carefully controlled by the optimization of slurry formulations of individual layers, and the cell fabrication was completed by co-firing the green-state cells in air at 1300–1330 °C for 2 h.

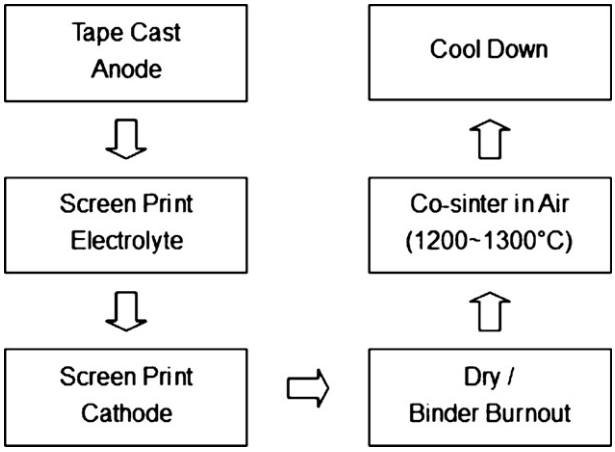

Fig. 1. Cell fabrication process.

2.3. Cell testing

Fig. 2 shows the schematic of a single cell test setup. It comprises of two alumina tubes, with the cell sandwiched between them. A gold gasket was placed on the cathode side, and a mica gasket was used on the anode side to seal and prevent direct contact between the cell and the ceramic tube. Glass paste was applied outside the tubes around the mating circumference to ensure a tight seal, and the assembled test setup was loaded into the furnace. Platinum or silver mesh was used as a current collector on the cathode side, and nickel mesh on the anode side. Platinum paste was applied between the cathode and the platinum or silver mesh, and nickel paste between the anode and the nickel mesh to ensure a good contact between the meshes and the electrodes. On each side, one wire was used as a current lead, and the other as a voltage-measurement lead. Humidified hydrogen was circulated over the anode, and air was circulated over the cathode. Electrochemical measurements were made with a Princeton Applied Research PARSTAT® 2273 potentiostat and impedance analyzer, and a KEPCO power amplifier over the temperature range from 700 °C to 800 °C.

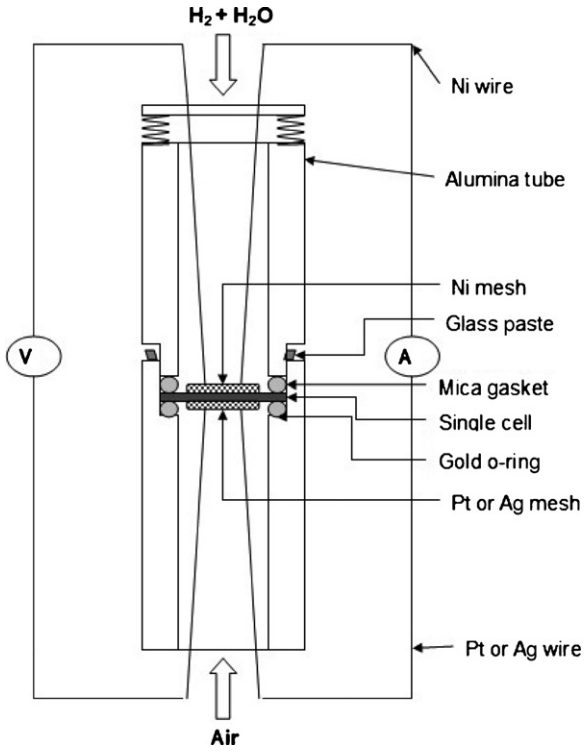

Fig. 2. A schematic of the single cell test setup.

2.4. Microstructural characterization

The cells were sectioned after testing, and they were impregnated with epoxy in vacuum. After the epoxy hardened, they were polished down to 1.0 μm, and the cross sections were examined using scanning electron microscopy (SEM). The porosities and the grain sizes of the electrodes were determined using the line intersection method.

3. Results and discussion

3.1. Polarization modeling

The operating cell potential (E_c) is always lower than the open circuit potential (E_0) due to various polarization losses, and the performance of the SOFC is determined by ohmic, activation, and concentration polarization. The operating cell potential can be expressed as [5]:

$$E_c = E_0 - iR_i - \eta_{act} - \eta_{a,conc} - \eta_{c,conc} \quad (1)$$

where i is the current density ($A\,cm^{-2}$), R_i the area specific ohmic resistance of the cell ($\Omega\,cm^2$), η_{act} the activation polarization (V), $\eta_{a,conc}$ the anodic concentration polarization (V), and $\eta_{c,conc}$ is the cathodic concentration polarization (V).

The area specific ohmic resistance of the cell, R_i, includes the ionic resistance of the electrolyte, the electronic resistances of the electrodes, and the contact resistances associated with all of the cell layer interfaces.

Activation polarization, η_{act}, is caused by slow charge transfer reactions at the electrocatalyst–electrolyte interfaces, and for small currents and/or rapid mass transfer, it is related to the current density, i, through the Butler–Volmer equation:

$$i = i_0 \exp\left(\frac{\alpha n \eta_{act} F}{RT}\right) - i_0 \exp\left(\frac{-(1-\alpha) n \eta_{act} F}{RT}\right) \quad (2)$$

where i_0 is an exchange current density, α the transfer coefficient, n the number of electrons transferred, and F is the Faraday's constant. Chen et al. have suggested that the transfer coefficient for fuel cell applications is 0.5 assuming a symmetric activation energy barrier for both electrode reactions [6]. The number of electrons transferred in the overall SOFC reaction, $H_2(g) + (1/2)O_2(g) = H_2O(g)$, is 2. However, the charge-transfer reaction rate can possibly be rate-controlled by the transfer of either one or two electrons. Thus, the number of electrons transferred per electrochemical reaction in the Butler–Volmer equation can be either one or two, depending on the reaction mechanism, and the value chosen in this paper was one because the polarization model indicated that it was a one-electron transfer reaction mechanisms, determined based on the best experimental fit of the results to the model. Therefore the charge-transfer reaction for the cells reported in this paper was considered to be rate-controlled by the transfer of one electron instead of two. It is interesting to note that n was also assumed to be 1 in the Butler–Volmer equation in prior work by Zhu and Kee [5]. If the values of $\alpha = 0.5$ and $n = 1$ are substituted into Eq. (2), the Butler–Volmer equation is expressed as:

$$i = i_0 \exp\left(\frac{\eta_{act} F}{2RT}\right) - i_0 \exp\left(-\frac{\eta_{act} F}{2RT}\right) \quad (3)$$

This equation can also be written in the form of a quadratic equation in the term $\exp(\eta_{act}F/2RT)$, i.e.

$$\left[\exp\left(\frac{\eta_{act} F}{2RT}\right)\right]^2 - \left(\frac{i}{i_0}\right)\left[\exp\left(\frac{\eta_{act} F}{2RT}\right)\right] - 1 = 0 \quad (4)$$

Solving this equation for $\exp(\eta_{act}F/2RT)$ gives

$$\exp\left(\frac{\eta_{act} F}{2RT}\right) = \frac{1}{2}\left[\left(\frac{i}{i_0}\right) + \sqrt{\left(\frac{i}{i_0}\right)^2 + 4}\right] \quad (5)$$

Thus, the relationship between the activation polarization and the current density can be expressed as [7]:

$$\eta_{act} = \frac{2RT}{F} \ln\left\{\frac{1}{2}\left[\left(\frac{i}{i_0}\right) + \sqrt{\left(\frac{i}{i_0}\right)^2 + 4}\right]\right\} \quad (6)$$

Concentration polarization of the cell, η_{conc}, occurs due to the slow mass transport of gas-phase reactant and/or product species through the porous anode and cathode. The electrode process can be dominated by the concentration polarization at high current densities and/or when the porosity is low or insufficient. This results in a convex-up curvature ($d^2V/di^2 < 0$) in the voltage versus current trace. If the electrode process is completely dominated by concentration polarization, limiting current is reached and the cell voltage drops rapidly. The anodic concentration polarization with H_2–H_2O gas mixture as fuel can be expressed

as [2,5]:

$$\eta_{a,conc} = -\frac{RT}{2F}\ln\left(\frac{p'_{H_2(i)}p^{\circ}_{H_2O}}{p^{\circ}_{H_2}p'_{H_2O(i)}}\right) = -\frac{RT}{2F}\ln\left(1-\frac{i}{i_{as}}\right) + \frac{RT}{2F}\ln\left(1+\frac{p^{\circ}_{H_2}i}{p^{\circ}_{H_2O}i_{as}}\right) \quad (7)$$

where R is the gas constant, F the Faraday constant, $p'_{H_2(i)}$ the partial pressure of hydrogen at the interface between the anode and electrolyte, $p'_{H_2O(i)}$ the partial pressure of water vapor at the interface between the anode and electrolyte, $p^{\circ}_{H_2(i)}$ and $p^{\circ}_{H_2O(i)}$ the partial pressure of hydrogen and water vapor in the anode bulk gas respectively, and i_{as} is the anodic limiting current density. When the current density is equal to the limiting current i_{as}, the interfacial hydrogen partial pressure $p'_{H_2(i)}$ is zero. Using this definition, i_{as} is given by [2]

$$i_{as} = \frac{2Fp^{\circ}_{H_2}D^{eff}_{H_2-H_2O}}{RTl_a} \quad (8)$$

where $D^{eff}_{H_2-H_2O}$ is the effective binary diffusivity of H_2 and H_2O in the anode, and l_a is the thickness of the anode.

The cathodic concentration polarization with air, which is a mixture of O_2 and N_2, can be expressed as [2,5]:

$$\eta_{c,conc} = -\frac{RT}{4F}\ln\left(\frac{p'_{O_2(i)}}{p^{\circ}_{O_2}}\right) = -\frac{RT}{4F}\ln\left(1-\frac{i}{i_{cs}}\right) \quad (9)$$

where $p'_{O_2(i)}$ is the partial pressure of oxygen at the interface between cathode and electrolyte, $p^{\circ}_{O_2}$ the partial pressure of oxygen in the cathodic bulk gas, and i_{cs} is the cathodic limiting current density. Analogous to the anode, when the current density equals the cathodic limiting current density i_{cs}, the interfacial oxygen partial pressure $p'_{O_2(i)}$ is zero. Using this definition i_{cs} is given by [2]

$$i_{cs} = \frac{4Fp^{\circ}_{O_2}D^{eff}_{O_2-N_2}}{(p-p^{\circ}_{O_2}/p)RTl_c} \quad (10)$$

where $D^{eff}_{O_2-N_2}$ is the effective binary diffusivity of O_2 and N_2 in the cathode, l_c the thickness of the cathode, and p is the total gas pressure in the cathode. Here, p was assumed to be constant (1 atm) due to the low utilization of air.

Finally, the relationship between the voltage and the current density is obtained by substituting Eqs. (6), (7) and (9) into Eq. (1):

$$E(i) = E_0 - iR_i - \frac{2RT}{F}\ln\left\{\frac{1}{2}\left[\left(\frac{i}{i_0}\right)+\sqrt{\left(\frac{i}{i_0}\right)^2+4}\right]\right\} + \frac{RT}{2F}\ln\left(1-\frac{i}{i_{as}}\right) - \frac{RT}{2F}\ln\left(1+\frac{p^{\circ}_{H_2}i}{p^{\circ}_{H_2O}i_{as}}\right) + \frac{RT}{4F}\ln\left(1-\frac{i}{i_{cs}}\right) \quad (11)$$

The experimental voltage versus current density traces from all the measurements were curve-fitted using Eq. (11), and R_i, i_0, i_{as}, and i_{cs} were treated as the fitting parameters.

3.2. Effect of electrolyte conductivity on the ohmic polarization

Zirconia-based oxides are the most widely used materials as SOFC electrolytes, and among them, YSZ is commonly used as an electrolyte in SOFCs. To improve the ionic conductivity of the electrolytes, scandia-stabilized zirconia can be employed, since it exhibits the highest ionic conductivity, which has been attributed to the low association enthalpy of the defect reactions and the similarity of the ionic radii of Sc^{3+} and Zr^{4+} [8–10]. For a successful single-step co-firing, it is very important to lower the sintering temperature of the electrolyte since the electrolyte should be fully densified while a sufficient porosity is maintained in the anode and the cathode. To lower the sintering temperature of the electrolyte, a sintering aid can be added to the electrolyte. However, the sintering aid should not degrade the electrical properties of the electrolyte and impair its function in the SOFC. Fig. 3 shows the results of the conductivity measurements of ScSZ and YSZ with and without sintering aid between 700 °C and 800 °C. The conductivity of ScSZ was 0.132 S cm^{-1} at 800 °C, 0.093 S cm^{-1} at 750 °C, and 0.061 S cm^{-1} at 700 °C without the sintering aid, and 0.161 S cm^{-1} at 800 °C, 0.099 S cm^{-1} at 750 °C, and 0.048 S cm^{-1} at 700 °C with the sintering aid. The conductivity of YSZ was 0.063 S cm^{-1} at 800 °C, 0.039 S cm^{-1} at 750 °C, and 0.023 S cm^{-1} at 700 °C without the sintering aid, and 0.050 S cm^{-1} at 800 °C, 0.031 S cm^{-1} at 750 °C, and 0.018 S cm^{-1} at 700 °C with the sintering aid. It shows that the conductivity of ScSZ is approximately twice that of YSZ, and the sintering aid did not have a significant effect on the conductivity of either YSZ or ScSZ. Fig. 4 compares the results of cell tests at 800 °C of two cells, one comprising ScSZ electrolyte and the other comprising YSZ electrolyte, both featuring the sintering aid, with humidified hydrogen (hydrogen bubbled through water at 25 °C) as fuel and air as oxidant. All the other processes and materials were maintained identical except for the electrolyte materials. Both cells were co-fired at 1330 °C, and Pt mesh was used for current collection on the cathode side, while

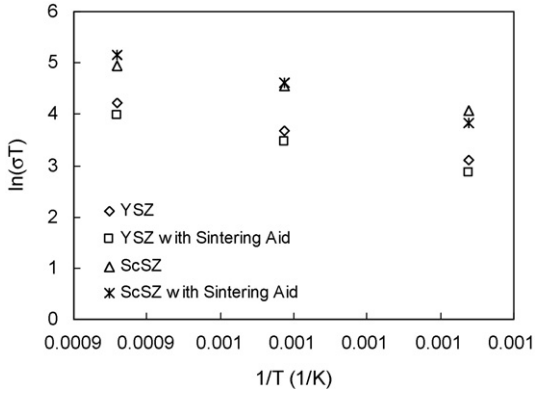

Fig. 3. Electrical conductivities of YSZ and ScSZ with and without sintering aid at 800 °C, 750 °C, and 700 °C.

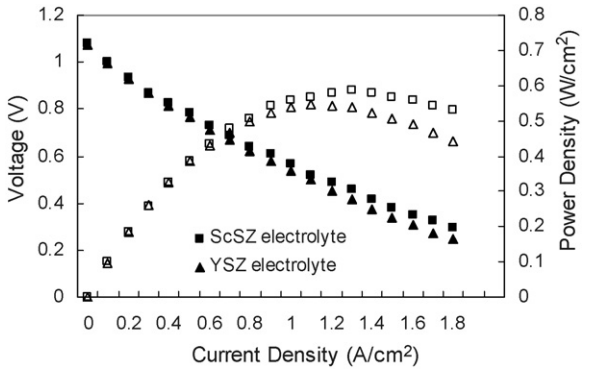

Fig. 4. Cell test results at 800 °C under humidified hydrogen and air for cells with different electrolyte materials, one with ScSZ and the other with YSZ.

Ni mesh was used on the anode side. The maximum power densities were 0.58 W cm^{-2} with ScSZ electrolyte, and 0.55 W cm^{-2} with YSZ electrolyte. The single cell test results did not show any significant difference in cell performance in spite of the higher ionic conductivity of ScSZ electrolyte. To analyze the contribution of various polarizations on the cell performance, the experimentally measured *I–V* curve was fitted to the polarization model described previously, and the fitting parameters including the total area specific ohmic resistance (R_i), exchange current density (i_0), anodic limiting current density (i_{as}), and cathodic limiting current density (i_{cs}) were obtained. The ohmic resistance (R_i) was separated into contributions from the electrolyte ($R_{electrolyte}$) and the electrode ($R_{electrode}$). The area specific resistance contribution of the electrolyte was calculated from the previously measured conductivity of each electrolyte material and the thickness of electrolyte layers. The remaining portion of the total ohmic resistance was considered to be the area specific resistance associated with the electrodes including the resistance of the cathode, anode, and the contact resistance of all the interfaces. The effective binary diffusivities of H_2 and H_2O in the anode ($D^{eff}_{H_2-H_2O}$) and those of O_2 and N_2 in the cathode ($D^{eff}_{O_2-N_2}$) were calculated from i_{as} and i_{cs} which were obtained from the fits using Eqs. (8) and (10). The results are shown in Table 1. Based on the curve fitting results combined with the estimate of the electrolyte contribution to the total area specific ohmic resistance obtained from the conductivity measurements, the ohmic loss due to the electrolyte, the ohmic loss associated with the electrodes, the activation polarization loss, and the anodic and cathodic concentration polarization losses were estimated as a function of current density using the previously described model in Eq. (11), and the results are plotted in Fig. 5. The YSZ electrolyte contribution is ∼12% of the total ohmic loss of the co-fired cell, and the ScSZ electrolyte contribution is ∼7% of the total ohmic loss. These results show that the ohmic contribution of the electrolyte is small compared to the ohmic contribution associated with the electrodes and the contacts, and the ohmic polarization of the cell is mainly dominated by the ohmic losses associated with the electrodes. An improvement in the cell performance over a YSZ electrolyte cell was not observed with the highly conductive electrolyte material since the electrolyte contribution to the overall cell polarization is insignificant. Therefore, although electrolyte materials exhibiting high ionic conductivity are desirable, it may not be an absolute necessity for SOFCs operating at ∼800 °C, especially for cells comprising thin electrolytes. The microstructure of the tested cell featuring the YSZ electrolyte is shown in Fig. 6. The anode support is ∼850 μm thick and ∼31% porous, the electrolyte is ∼15 μm thick, the cathode active layer is ∼33 μm thick and ∼31% porous, and the cathode current collector is ∼54 μm thick and 48% porous. The thicknesses and porosities of the various layers of the tested cell featuring ScSZ electrolyte are nearly identical. SEM images of the electrolyte layers of these two cells in Fig. 7 show that YSZ electrolyte is fully densified while ScSZ electrolyte contains many micro-pores. As mentioned before, it is very important to fully densify the electrolyte at a low sintering temperature for successful implementation of the single step co-firing process. Therefore, the YSZ electrolyte with the sintering aid is considered to be a more satisfactory electrolyte than the ScSZ from the stand point of cell fabrication: thus all the subsequent cells in the experiments described below featured a YSZ electrolyte with the sintering aid.

Table 1
Curve fitting results of the cells with ScSZ and YSZ electrolyte tested at 800 °C under humidified hydrogen and air

Fitting parameters	Cell with ScSZ electrolyte	Cell with YSZ electrolyte
R_i (Ω cm^{-2})	0.16	0.18
$R_{electrolyte}$ (Ω cm^{-2})	0.011 (7%)	0.024 (14%)
$R_{electrode}$ (Ω cm^{-2})	0.149 (93%)	0.156 (86%)
i_0 (mA cm^{-2})	398	371
i_{as} (A cm^{-2})	3.20	2.99
$D^{eff}_{H_2-H_2O}$ (cm^2 s^{-1})	0.127	0.120
i_{cs} (A cm^{-2})	3.07	2.16
$D^{eff}_{O_2-N_2}$ (cm^2 s^{-1})	0.021	0.016

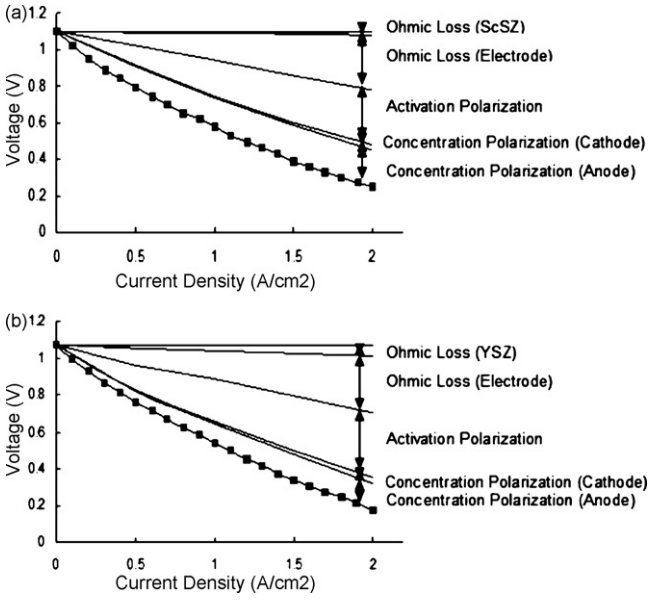

Fig. 5. Separation of the polarization losses by modeling on cells (a) with ScSZ electrolyte and (b) with YSZ electrolyte.

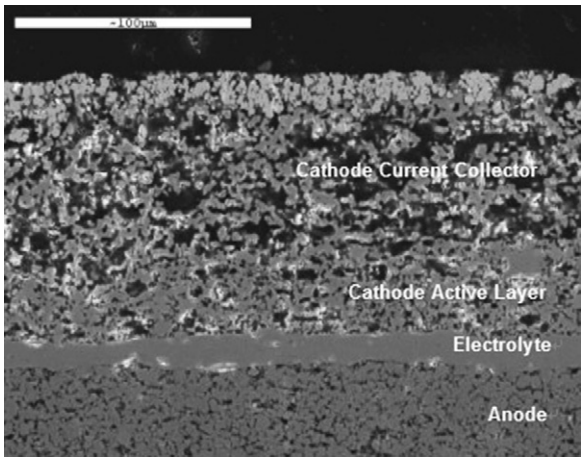

Fig. 6. SEM micrograph of the tested cell with YSZ electrolyte.

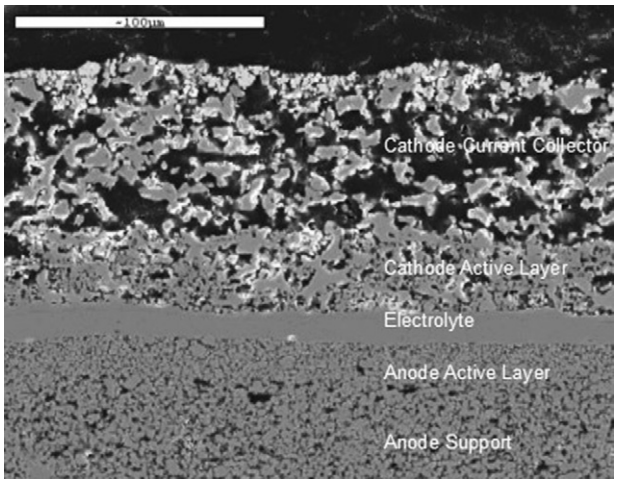

Fig. 8. SEM image of the cell with anode active layer.

3.3. Effect of anode active layer on the activation polarization

Activation polarization occurs due to slow electrode kinetics, and the relationship between activation polarization and the current density is expressed by the Butler–Volmer Eq. (2). As used in this paper, the Butler–Volmer equation, the net activation polarization contributions of both the cathode and the anode are lumped together. Since the activation polarizations from both electrodes are lumped into one single polarization equation, the contribution of each electrode needs to be determined experimentally. The activation polarization is dependent on the number of reaction sites which are attributed to the triple phase (gas–electrode–electrolyte) boundary (TPB) length in porous, two phase mixed conducting electrodes. In the anode, the boundary between nickel and zirconia particles works as the TPBs, and the anodic activation polarization can be reduced by having an anode active layer greater than a certain critical thickness, finer microstructures and longer TPB length. The anode active layer shown in Fig. 8 has such a structure and thickness. The anode active layer is 17 μm thick and 25% porous. Therefore, it was expected that the anode active layer would improve the electrochemical performance on the anode side due to an increase in the number of effective reaction sites. Fig. 9 shows the results of cell tests of two cells, one with an anode active layer and the other without an anode active layer, measured at 800 °C with humidified hydrogen (hydrogen bubbled through water at 25 °C) and air. All the other fabrication processes and materials were maintained identical between the two cells except for the anode active layer. Both cells were co-fired at 1330 °C, and Pt mesh was used for current collection on the cathode side, while Ni mesh was

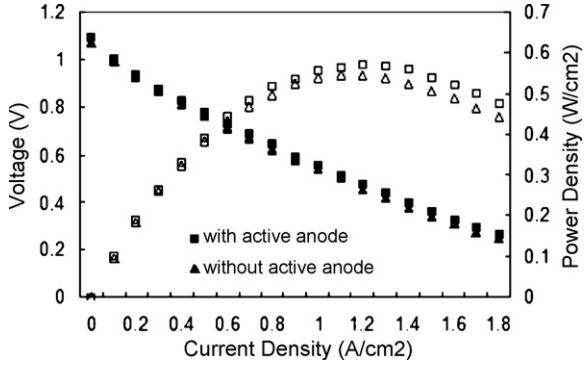

Fig. 9. Cell test results at 800 °C under humidified hydrogen and air for cells with and without anode active layer.

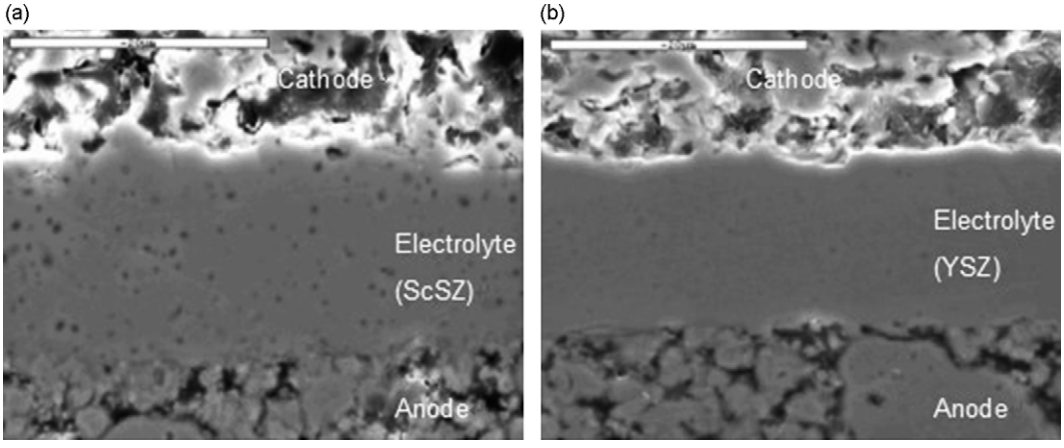

Fig. 7. SEM micrographs of the cells with (a) ScSZ electrolyte and (b) YSZ electrolyte.

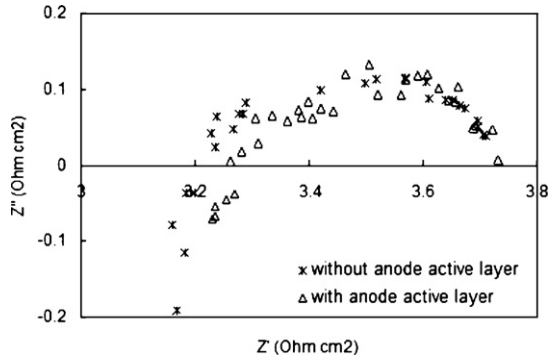

Fig. 10. Impedance spectroscopy measurements at open circuit potential for two cells, one with anode active layer and the other without anode active layer, under humidified hydrogen and air at 800 °C.

used on the anode side. The maximum power density of the cell with the anode active layer was 0.57 W cm^{-2}, and that of the cell without the anode active layer was 0.55 W cm^{-2}. In this experiment, significant enhancement in the cell performance was not observed by employing the anode active layer. Fig. 10 shows the results of impedance spectroscopy under open circuit conditions for these two cells with humidified hydrogen (hydrogen bubbled through water at 25 °C) and air at 800 °C. As described in prior work [11–15], the low frequency intercept corresponds to the total polarization resistance including ohmic resistance, activation polarization resistance, and concentration polarization resistance. The high frequency intercept corresponds to the ohmic resistance of the cell. Therefore, the sum of the activation and concentration polarization resistances can be obtained by subtracting the high frequency intercept from the low frequency intercept. The polarization resistance of the cell with an anode active layer was 0.52 Ω cm^{-2}, which was of the same order of magnitude as that of the cell without the anode active layer, 0.51 Ω cm^{-2}. In addition, there was no improvement in the estimated exchange current density obtained as shown in Table 2. The exchange current density represents the net rate of electrode processes, and it can be directly related to the activation polarization of the cathode and the anode. Therefore, it is concluded that the majority of the activation polarization loss occurs due to the slow charge transfer reaction in the cathode, and the contribution of the anode to the net activation polarization is insignificant under the usual test conditions. However, preliminary experiments of the effect of anode gas composition reveal that the anodic activation polarization becomes significant as water vapor composition in the fuel increases. The maximum power density drops from 1.5 W cm^{-2} to 0.5 W cm^{-2} as water vapor composition in fuel increases from 3% to 70%. Therefore, the effect of anode active layer becomes more significant at high fuel utilization conditions, although it was not obvious under the present test condition (97% H_2–3% H_2O). These effects will be published in a forthcoming paper.

Table 2
Curve fitting results of the cells with and without anode active layer tested at 800 °C under humidified hydrogen and air.

Fitting parameters	Cell with active anode	Cell without active anode
R_i (Ω cm^{-2})	0.18	0.18
$R_{electrolyte}$ (Ω cm^{-2})	0.024 (14%)	0.024 (14%)
$R_{electrode}$ (Ω cm^{-2})	0.156 (86%)	0.156 (86%)
i_0 (mA cm^{-2})	344	371
i_{as} (A cm^{-2})	2.72	2.99
$D^{eff}_{H_2-H_2O}$ (cm^2 s^{-1})	0.109	0.120
i_{cs} (A cm^{-2})	2.89	2.16
$D^{eff}_{O_2-N_2}$ (cm^2 s^{-1})	0.020	0.016

3.4. Effect of contact resistance on the ohmic polarization

Jiang showed that the contact resistance between the electrode and current collector can contribute significantly to the total cell resistance in SOFCs [16]. In our previous polarization analysis, it was shown that the contribution of the electrodes to the total ohmic loss is much greater than that due to the electrolyte. The ohmic resistance associated with electrodes contains both electrode resistance and contact resistance, and they can be separated by estimation of the electrode resistance. The conductivity of LCM was measured to be 89 S cm^{-1} at 800 °C. The conductivity of the cathode active layer can be roughly estimated as:

$$\sigma_{CAL} = V_{LCM}\sigma_{LCM} + V_{YSZ}\sigma_{YSZ} \quad (12)$$

where σ_{CAL}, σ_{LCM}, and σ_{YSZ} are the conductivities of cathode active layer, LCM, and YSZ, respectively, and V_{LCM} and V_{YSZ} are the volume fractions of LCM, and YSZ, respectively. The conductivity of the cathode active layer is calculated to be ~29 S cm^{-1} and the area specific resistance of a 30 μm thick cathode active layer is about 0.00010 Ω cm^{-2}. In a similar manner, the area specific resistance of 50 μm thick cathode current collector layer is about 0.00012 Ω cm^{-2}. The conductivity of Ni-YSZ anode cermet was reported to be ~1200 S cm^{-1} at 800 °C [17], and the area specific resistance of 850 μm thick anode is calculated to be 0.00007 Ω cm^{-2}. Therefore, the total electrode resistance including the cathode active layer, the cathode current collector, and the anode is 0.00029 Ω cm^{-2}. This is less than 15% of the ohmic resistance associated with electrode. Since the geometric factors related to the electrode microstructures such as neck formation and connectivity of the conducting phases were not considered in the estimation of cathode resistance, the actual electrode resistance is expected to be somewhat higher than the calculated value. However, it is obvious that the contact resistance contribution is much larger than the contribution of the electrode in the overall ohmic loss associated with the electrode.

According to Meulenberg et al. [18], Ag meshes are stable current collectors on the cathode side for SOFC operation temperatures up to 800 °C. Therefore, the effect of lowering the contact resistance between the cathode and the current collector on the overall cell performance was evaluated using Ag mesh on one cell and Pt mesh on the other cell. In both cases, Pt paste was applied between the mesh and the electrode to ensure good electrical contact. Fig. 11 shows the cell test results wherein the current collection method was varied. Pt mesh was used for one cell on the cathode for the current collection, and Ag mesh was

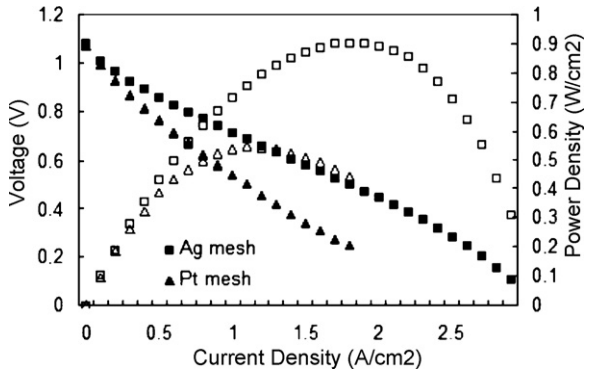

Fig. 11. Cell test results at 800 °C under humidified hydrogen and air for cells measured with Pt mesh and Ag mesh for the cathode current collection.

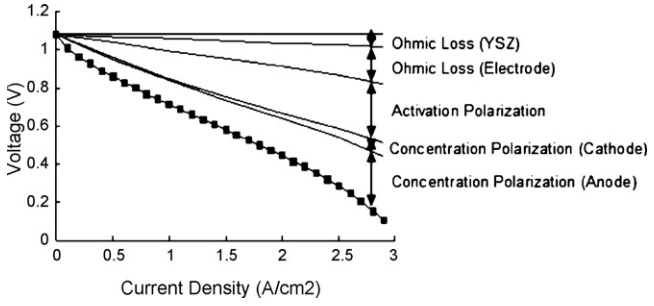

Fig. 12. Separation of the polarization losses by modeling on cells measured with Ag mesh for the cathode current collection.

used for the other cell for the cathode current collection. All the other processes and materials were maintained identical and both cells were co-fired at 1330 °C. These cells were tested at 800 °C under humidified hydrogen (hydrogen bubbled through water at 25 °C) and air. The maximum power density of the cell measured with Pt mesh on the cathode side was 0.55 W cm^{-2}, and the maximum power density of the cell measured with Ag mesh on the cathode side was 0.91 W cm^{-2}. The maximum power density obtained with Ag mesh was about 40% higher than that with Pt mesh. Fig. 12 shows that the contribution of the electrode ohmic loss to the total ohmic loss decreased from 86% to 65% by employing Ag mesh as the current collector instead of Pt. This result can be rationalized on the premise that the

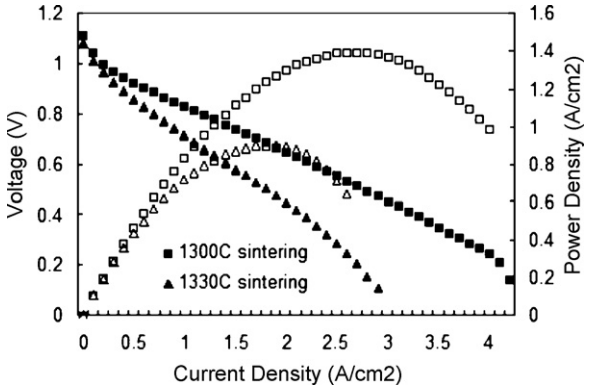

Fig. 13. Cell test results at 800 °C under humidified hydrogen and air for cells sintered at 1330 °C and 1300 °C.

different melting temperatures and softening behaviors of Ag and Pt lead to different extents of adhesion of the current collector to the cathode. The melting temperature of Ag is 961 °C, and it is significantly lower than that of Pt (1772 °C). The cell operating temperature of 800 °C is 0.87 times the melting temperature of Ag, and 0.53 times that of Pt. Thus, Ag is expected to be softer than Pt at the operating temperature, which leads to a higher interfacial contact area between the cathode and the current collector, thus lowering the contact resistance. In SOFC stacks, individual cells are connected by interconnects, and the overall stack performance is dependent not only on the performance of the individual cells but also on the contact between the electrode and the interconnect materials. The significant improvement of the cell performance by improving the electrical contact observed in this experiment indicates that the effect of the contact between the electrode and the interconnect on the performance of the SOFC stack can be substantial.

3.5. Effect of cathode microstructure on the activation polarization

In the previous experiment on the anode active layer, it was shown that the majority of the activation polarization loss occurs on the cathode side. Since the sintering temperature strongly affects the microstructures and TPBs of the cathode active layer, it is a very important processing parameter that influences the

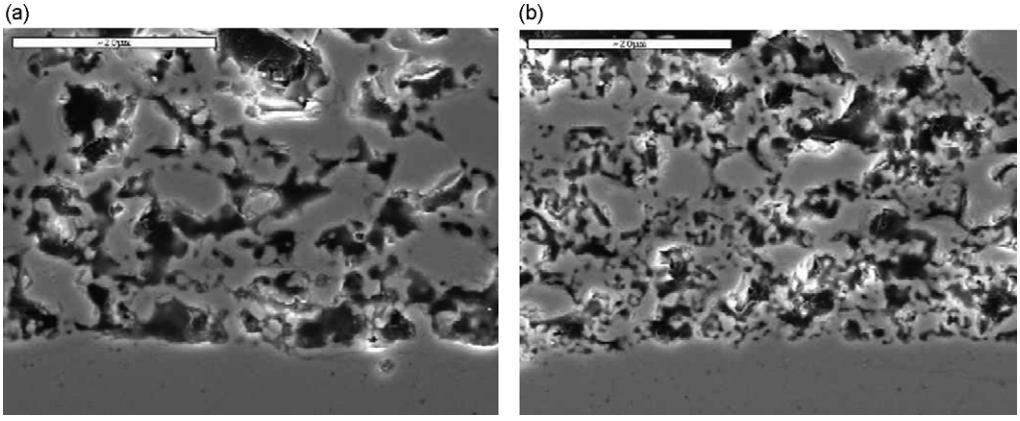

Fig. 14. SEM micrographs of the cathode active layers of two cells: (a) fired at 1330 °C and (b) fired at 1300 °C.

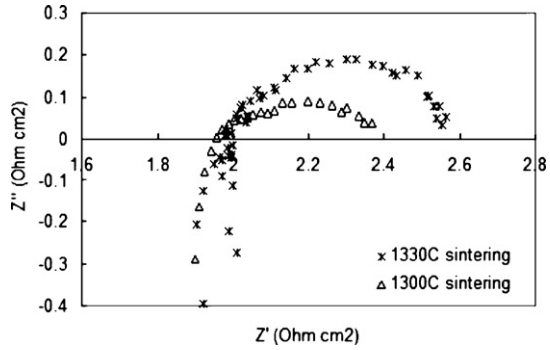

Fig. 15. Impedance spectroscopy measurements at open circuit potential for cells sintered at 1330 °C and 1300 °C.

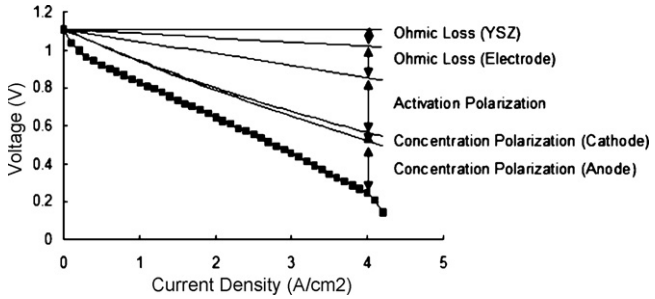

Fig. 16. Separation of the polarization losses by modeling on a cell sintered at 1300 °C and measured with Ag mesh for the cathode current collection.

cathodic activation polarization [19]. Fig. 13 shows the cell test results of two cells fired at different temperatures. One of them was fired at 1330 °C, and the other at 1300 °C. All the other processes and materials were maintained identical except for the sintering temperature. Ag mesh was used for current collection on the cathode as before, and Ni mesh was used on the anode. These cells were tested at 800 °C under humidified hydrogen (hydrogen bubbled through water at 25 °C) and air. The maximum power density of the cell fired at 1330 °C was 0.91 W cm^{-2}, while that of the cell fired at 1300 °C was 1.40 W cm^{-2}. Lowering the sintering temperature by 30 °C (from 1330 °C to 1300 °C) improved the maximum power density by 54% (from 0.91 W cm^{-2} to 1.40 W cm^{-2}) at 800 °C under humidified hydrogen (hydrogen bubbled through water at 25 °C) and air. Fig. 14 shows the microstructures of the cathode active layer of these two cells. The average grain size of the cathode active layer of the cell fired at 1330 °C was 3.13 μm, while that of the cell fired at 1300 °C was somewhat smaller at 2.32 μm. The average grain size of the anode of the cell fired at 1330 °C was 2.17 μm, and that of the cell fired at 1300 °C was 2.09 μm. Therefore, decreasing the sintering temperature has a more significant effect on the microstructure of the cathode active layer than that of the anode. Sintering is a process driven by solid state interdiffusion. In composite electrodes with multiple phases which also include a pore phase, it is difficult to make comparisons of interdiffusion coefficients. However, it is interesting to note that the observed results are consistent with the higher melting temperature of NiO (1960 °C) than $LaMnO_3$ (1880 °C), since it is generally known that interdiffusion coefficients scale with melting temperature. It has been theoretically shown by Tanner et al. that the effective charge-transfer resistance scales as the square root of the grain size of the electrode material [20]. Thus, the grain size of the cathode active layer becomes smaller as the sintering temperature is lowered, and this increases the active TPB length between LCM, YSZ, and the gas phase, leading to a lower activation polarization in the cathode. This was also verified by the impedance spectroscopy data as shown in Fig. 15. The polarization resistance of the cell fired at 1330 °C was 0.58 Ω cm^{-2}, and that of the cell fired at 1300 °C was 0.39 Ω cm^{-2}. Fig. 16 shows the polarization losses in the cell fired at 1300 °C. It is clearly evident that the exchange current density has increased and the activation polarization has been reduced due to the improvement of microstructures of the cathode active layer by lowering the sintering temperature (Table 3).

3.6. Effect of anode porosity on the concentration polarization

The binary diffusivity of hydrogen and water vapor is much higher than that of oxygen and nitrogen due to the lower molecular weight of the hydrogen–water vapor mixture compared to a mixture of oxygen–nitrogen. The diffusivities obtained from the curve fits also confirmed that the effective binary diffusivity of hydrogen and water vapor in the anode is about an order of magnitude higher than that of oxygen and nitrogen in the cathode. However, since the anode (∼850 μm thick) is much thicker than the cathode (∼80 μm thick) in anode supported SOFCs, the contribution of the anode concentration polarization is higher than that of the cathode, which has been clearly shown in the de-convolution of the polarization losses by curve fitting in Fig. 16. Especially at high current density, the contribution of the anode concentration polarization to the overall voltage losses is not negligible. The effective binary diffusivity of the reactant and product gases in the thick porous anode is affected by the microstructural parameters of the anode such as volume fraction of pores and tortuosity, and the gas phase mass transfer can be enhanced by increasing the porosity in the anode. The anode porosities of the cells tested previously were maintained at ∼31%; however the porosity can be increased by the addition of a pore former. Fig. 17 compares test results of cells with anode porosity of 31% and 37%. All the other processes and materials were maintained identical except for the anode porosity, and both cells were fired at 1300 °C. Ag mesh

Table 3
Curve fitting results of the cells fired at 1300 °C and 1330 °C tested at 800 °C under humidified hydrogen and air

Fitting parameters	Cell fired at 1300 °C	Cell fired at 1330 °C
R_i (Ω cm^{-2})	0.06	0.08
$R_{electrolyte}$ (Ω cm^{-2})	0.024 (40%)	0.024 (30%)
$R_{electrode}$ (Ω cm^{-2})	0.036 (60%)	0.056 (70%)
i_0 (mA cm^{-2})	878	567
i_{as} (A cm^{-2})	4.13	2.90
$D^{eff}_{H_2-H_2O}$ (cm^2 s^{-1})	0.164	0.116
i_{cs} (A cm^{-2})	4.68	2.91
$D^{eff}_{O_2-N_2}$ (cm^2 s^{-1})	0.032	0.020

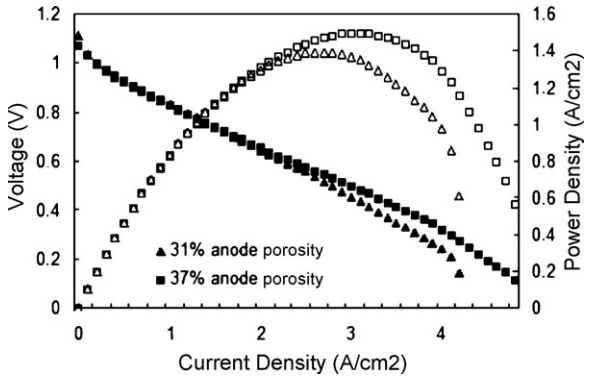

Fig. 17. Cell test results at 800 °C under humidified hydrogen and air for cells with 31% anode porosity and 37% anode porosity.

was used for current collection on the cathode, and Ni mesh was used on the anode as before. These cells were tested at 800 °C under humidified hydrogen (hydrogen bubbled through water at 25 °C) and air. The maximum power density of the cell with 31% anode porosity was 1.40 W cm^{-2}, while that of the cell with 37% anode porosity was 1.50 W cm^{-2}. The impedance spectroscopy data in Fig. 18 shows that the polarization resistance of the cell with 31% anode porosity was 0.39 Ω cm^{-2}, and that of the cell with 37% anode porosity was 0.21 Ω cm^{-2}. According to Kim et al., the effect of concentration polarization persists at a very low current density, and it is not negligible even close to the open-circuit limit [2]. Impedance spectroscopy measurements were performed at open circuit potential, and it shows significant improvement in polarization resistance with increased anode porosity. The cathode microstructures of the two cells were essentially the same, therefore it is concluded that the anodic concentration polarization contributes significantly to the polarization resistance even under very low current density conditions. Table 4 shows the curve fitting results. The effective binary diffusivity of hydrogen and water vapor of the cell with 31% anode porosity is 0.164 cm^2 s^{-1}, while that of the cell with 37% anode porosity is 0.197 cm^2 s^{-1}. The effective binary diffusivity is a function of porosity and tortuosity of the electrode:

$$D^{\text{eff}}_{\text{A-B}} = \frac{V}{\tau} D_{\text{A-B}} \tag{13}$$

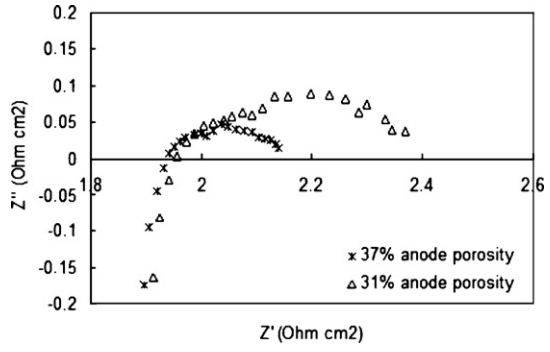

Fig. 18. Impedance spectroscopy measurements at open circuit potential for cells with 31% anode porosity and 37% anode porosity.

Table 4
Curve fitting results of the cells with 31% anode porosity and 37% anode porosity tested at 800 °C under humidified hydrogen and air

Fitting parameters	Cell with 37% porous anode	Cell with 31% porous anode
R_i (Ω cm^{-2})	0.05	0.06
$R_{\text{electrolyte}}$ (Ω cm^{-2})	0.024 (48%)	0.024 (40%)
$R_{\text{electrode}}$ (Ω cm^{-2})	0.026 (52%)	0.036 (60%)
i_0 (mA cm^{-2})	1090	878
i_{as} (A cm^{-2})	4.97	4.13
$D^{\text{eff}}_{\text{H}_2-\text{H}_2\text{O}}$ (cm^2 s^{-1})	0.197	0.164
i_{cs} (A cm^{-2})	4.35	4.68
$D^{\text{eff}}_{\text{O}_2-\text{N}_2}$ (cm^2 s^{-1})	0.030	0.032

where V is porosity and τ is tortuosity. Therefore, the effective binary diffusivity is proportional to the porosity of the electrode. In this experiment, the increase of anode porosity by 19% from 31% to 37% (((37 − 31)/31) × 100 = 19%) is consistent with the 20% increase in the effective binary diffusivity of the anode obtained from the polarization model: effective binary diffusivity increased from 0.164 cm^2 s^{-1} to 0.197 cm^2 s^{-1}. This result also validates the polarization model used in this work.

Figs. 19 and 20 shows *I–V* curves and power density data of the cell with 37% anode porosity measured at 800 °C, 750 °C, and 700 °C with humidified hydrogen and air. The maximum power densities were 1.50 W cm^{-2} at 800 °C, 1.20 W cm^{-2} at 750 °C, and 0.87 W cm^{-2} at 700 °C.

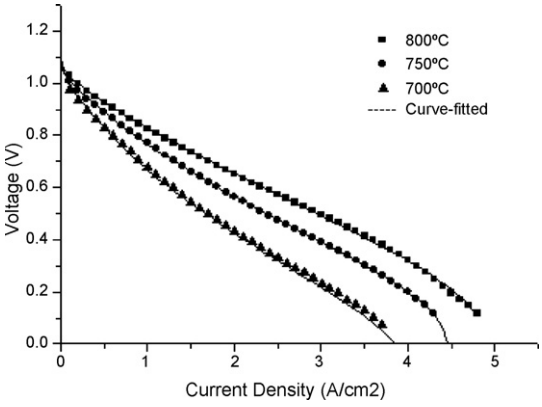

Fig. 19. *I–V* curves of the cell with 37% anode porosity measured at 800 °C, 750 °C, and 700 °C with humidified hydrogen and air.

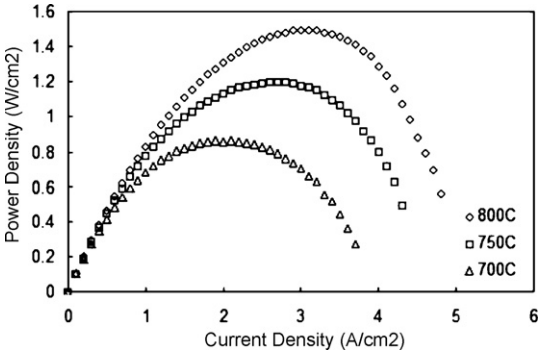

Fig. 20. Power density curves of the cell with 37% anode porosity measured at 800 °C, 750 °C, and 700 °C with humidified hydrogen and air.

4. Conclusions

In this work, anode-supported planar solid oxide fuel cells were successfully fabricated by a single step co-firing process. The fabrication process involved tape casting of the anode, screen printing of the electrolyte and the cathode, and co-firing of the green-state cell at 1300–1330 °C for 2 h. The cells comprised of a Ni + YSZ anode, a YSZ electrolyte, an LCM + YSZ composite cathode active layer, and an LCM cathode current collector layer. Cells were tested in the temperature range between 700 °C and 800 °C under humidified hydrogen and air, and the effects of several parameters on the overall cell performance were studied using a suitable polarization model. It was shown that the ohmic resistance associated with the contacts and the cathodic activation polarization is the dominant factor that limits the cell performance under the test conditions. The contact resistance was improved by the use of Ag mesh instead of Pt mesh for the current collection on the cathode side. The cathodic activation polarization can be reduced even further by the improvement of the microstructure of the cathode active layer through lowering the sintering temperature. Further, improvement in the cell performance was achieved by increasing anode porosity and reducing anode concentration polarization. As a result, the maximum power density of 1.5 W cm^{-2} was obtained at 800 °C under humidified hydrogen and air. To date, this is the highest single cell power density reported on a cell fabricated in a single high temperature firing step. Further improvement of the cell performance can be expected by optimizing the electrode microstructure and composition.

Acknowledgements

This work was financially supported by BTU international. The authors wish to thank Dr. Guosheng Ye, Mr. Donald A. Seccombe, Jr. and Mr. Wenhua Huang for useful discussions.

References

[1] S. de Souza, S.J. Visco, L.C. De Jonghe, Solid State Ionics 98 (1997) 57.
[2] J.W. Kim, A.V. Virkar, K.Z. Fung, K. Mehta, S.C. Singhal, J. Electrochem. Soc. 146 (1999) 69.
[3] F. Zhao, A.V. Virkar, J. Power Sources 141 (2005) 79.
[4] K.J. Yoon, S. Gopalan, U.B. Pal, Mater. Res. Soc. Symp. Proc. 972 (2007), 0972-AA10-02.
[5] H. Zhu, R.J. Kee, J. Power Sources 117 (2003) 61.
[6] S.H. Chan, K.A. Khor, Z.T. Xia, J. Power Sources 93 (2001) 130.
[7] P.W. Li, M.K. Chyu, J. Heat Transfer 127 (2005) 1344.
[8] D. Lee, L. Lee, Y. Jeon, R. Song, Solid State Ionics 176 (11/12) (2005) 1021.
[9] M. Okamoto, Y. Akimune, K. Furuya, M. Hatano, M. Yamanaka, M. Uchiyama, Solid State Ionics 176 (7/8) (2005) 675.
[10] C. Varanasi, C. Juneja, C. Chen, B. Kumar, J. Power Sources 147 (1/2) (2005) 128.
[11] J.E. Bauerle, J. Phys. Chem. Solids 30 (1969) 2657.
[12] V.V. Krishnan, S. McIntosh, R.J. Gorte, J.M. Vohs, Solid State Ionics 166 (2004) 191.
[13] S. McIntosh, J.M. Vohs, R.J. Gorte, J. Electrochem. Soc. 150 (2003) A1305.
[14] A. Barbucci, R. Bozzo, G. Cerisola, P. Constamagna, Elecrochem. Acta 47 (2002) 2183.
[15] R. Macdonald, Impedance Spectroscopy: Emphasizing Solid Materials and Systems, Wiley, New York, 1987.
[16] S.P. Jiang, J. Electrochem. Soc. 148 (2001) A887.
[17] T. Ota, M. Koyama, C. Wen, K. Yamada, H. Takahashi, J. Power Sources 118 (2003) 430.
[18] W.A. Meulenberg, O. Teller, U. Glesch, H.P. Buchkremer, D. Stover, J. Mater. Sci. 36 (2001) 3189.
[19] M.J. Jorgensen, S. Primdahl, C. Bagger, M. Mogensen, Solid State Ionics 139 (2001) 1.
[20] C.W. Tanner, K.Z. Fung, A.V. Virkar, J. Electrochem. Soc. 1 (1997) 21.